



Energy harvesting from a thin polymeric film based on PVDF-HFP and PMMA blend

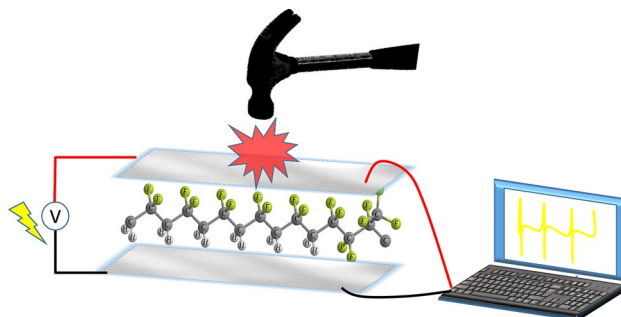
Kinyas Polat¹

Received: 23 April 2020 / Accepted: 2 June 2020 / Published online: 8 June 2020
© Springer-Verlag GmbH Germany, part of Springer Nature 2020

Abstract

Herein, a thin polymeric film prepared by spin coating technique using the blend of poly(vinylidene fluoride-co-hexafluoropropylene) (PVDF-HFP) and poly(methyl methacrylate) PMMA (1:1 mixing ratio) was introduced and compared with the pure PVDF-HFP. SEM, XRD, FTIR, TGA and DSC characterizations were conducted. Piezoelectric response was measured by hand made setup and the produced signal measured by a digital oscilloscope. Blending with PMMA increased the β -phase content, improved the heat stability. Crystallization point decreased from 140 to 129 °C and glass transition temperature changed from 59 to 94 °C. A uniform porous film structure was obtained with a thickness value of 12 μm . Piezoelectric potential obtained by applying mechanical force was found 4.385 V and 8.101 V for pure PVDF-HFP and the blend film, respectively. 84.7% increase found in the piezoelectric potential could be a promising result for energy harvesting and sensors applications.

Graphic abstract



Keywords Piezoelectricity · PVDF-HFP · PMMA · Isotactic · Syndiotactic · β Phase

1 Introduction

Energy harvesting is defined as capturing or scavenging energy from the surround by using various techniques to supply energy especially for the battery powered devices where charging or replacement of the battery is inefficient. From daily life usage to medical or military applications, such as pressure monitoring systems, implanted sensor nodes,

unmanned vehicles, running military security systems, the importance of energy harvesting is increasing day by day [1]. With the growth of microelectromechanical system (MEMS) technologies, micro energy harvesting has become more and more focus of the researches in the recent decade. Some of the micro energy harvesting sources are motion, vibration (or mechanical energy), object's movement, pavement, stairs etc. Energy harvesting from these sources can be achieved by electromagnetic, electrostatic, piezoelectric transducers and triboelectric generators which is based on contact electrification between two different layers [2–6]. Piezoelectric materials can be divided into two class as piezoceramics

✉ Kinyas Polat
kinyas.polat@deu.edu.tr

¹ Department of Chemistry, Faculty of Science, Dokuz Eylul University, 35390 Izmir, Turkey

and piezopolymers. Although piezoceramics produce high voltage output, they are brittle and not suitable for most applications. On the other hand, piezopolymers are flexible materials with enough voltage output but not as much as piezoceramics. Mechanical flexibility and processability into different shapes makes the piezopolymers very attractive materials for the researchers [7]. As being one of the most important piezopolymeric material, poly(vinylidene fluoride) (PVDF) is a very special polymer having high chemical and mechanical strength to be used in some special fields such as transducers, biomedical applications, optoelectronics [8–18]. Poly(vinylidene fluoride-co-hexafluoropropylene) (PVDF-HFP), a copolymer of PVDF containing extra fluor atoms on the side backbone, is a more hydrophobic and less crystalline alternative [19–22]. Piezoelectric property of the PVDF-HFP is generally associated with its crystal orientation in which fluor atoms bonded to carbon atoms create dipole moment. When the dipoles are forced to be positioned parallel to each other and all in the same direction, an increased piezoelectricity is observed. PVDF has several crystal orientation called as α -phase, β -phase, γ -phase, δ -phase [23]. The only electrically inactive non-polar phase is α -phase [24]. Piezoelectricity, conversion of mechanical energy to electrical and electrical energy to mechanical energy, can be more efficiently achieved by increasing the β -phase content of PVDF and PVDF-HFP polymers. Therefore, many research activities targeted to enhance the β -phase of these polymers by making their nano-forms, composites by electrospinning, nanocomposite producing methods, using multilayer materials (intercalating materials) such as montmorillonite, 3D printing, graphene and carbon nanotube incorporation, metallic nanoparticle incorporation [25–31]. Apart from all the above methods, there is another efficient but least benefited method to increase the β -phase content of PVDF polymers. In this method, a carbonyl group containing polymer is blended with the polymer based on the dipole–dipole interactions between carbonyl and polar fluor groups but the applications of such blends merely directed to piezoelectricity but rather ultra-filtration membranes or lithium batteries were focused on instead [32–37]. In a study that was recently carried out, PVDF-HFP was blended with polymethylmethacrylate (PMMA) (42.6% by volume) and corresponding energy storage capacity was determined. It was shown that incorporation of PMMA induced the γ -phase in a ratio of 93.6% [38]. In another study carried out by Zhu et al. PVDF-HFP polymer was blended with PMMA (10% by weight) and an increase in β -phase content was observed but above this amount no additional change in the β -phase was seen. Also decreasing quench temperature was found to be effective on the formation of β -phase [33].

In all of these studies, piezoelectric response of the blends was not tested. In this study, PVDF-HFP polymer was blended with PMMA with equal amounts and converted to

thin films by spin coating technique. The reason for increase in β -phase composition of PVDF-HFP when blended with poly (methyl methacrylate) (PMMA) was explained in terms of tacticity of PMMA for the first time. Piezoelectric response was measured by hand-made mechanical setup and the signals were followed by a digital oscilloscope.

2 Materials and methods

2.1 Reagents

Poly(methyl methacrylate) (PMMA) was purchased from Sigma with an average molecular weight of 350,000 g/mol. Poly(vinylidene fluoride-co-hexafluoropropylene) (PVDF-HFP) was purchased from Sigma (M_w : 455,000 g mol⁻¹, M_n : 110,000 g mol⁻¹). THF and DMF were purchased from Sigma.

2.2 Preparation method

Polymer blend was prepared from a solution of 10 g of PMMA and PVDF-HFP polymers in a 100 mL mixture of THF-DMF (1:1). The solution was converted into 12 μ m thick films by a spin-coater at 4000 rpm rotation speed.

2.3 Characterization

Prepared films of pure PVDF-HFP and a blend of PVDF-HFP and PMMA were characterized by Carl Zeiss 300VP SEM scanning electron microscope (SEM), Panalytical Empyrean XRD, TA Q2000 thermogravimetric analyser (TGA) and differential scanning calorimeter (DSC), fourier transform Nicolet iS50R infrared spectrometer (FTIR). Piezoelectric response of the films, which were sandwiched with two conductive flexible electrodes, was measured by Instrustar ISDS205B digital oscilloscope.

3 Results and discussions

3.1 Evaluation of phases with FTIR

FTIR spectrometer with ATR setup was used to identify the crystalline phases of the films. FTIR-ATR spectrum of the pure PVDF-HFP film and its blend form are given in Figs. 1 and 2. The absorption peaks at 841 cm⁻¹ and 1431 cm⁻¹, 1436 cm⁻¹ were attributed to the β -phase of PVDF HFP, those peaks at 1401 cm⁻¹, 1402 cm⁻¹, 615 cm⁻¹, 605 cm⁻¹ and 495 cm⁻¹, 481 cm⁻¹ were assigned to the α -phase [39]. The peaks at 841 cm⁻¹ and 1431 cm⁻¹ are special to the β -phase of PVDF HFP and intensities of these peaks are raise up when blended with PMMA as shown in Fig. 2.

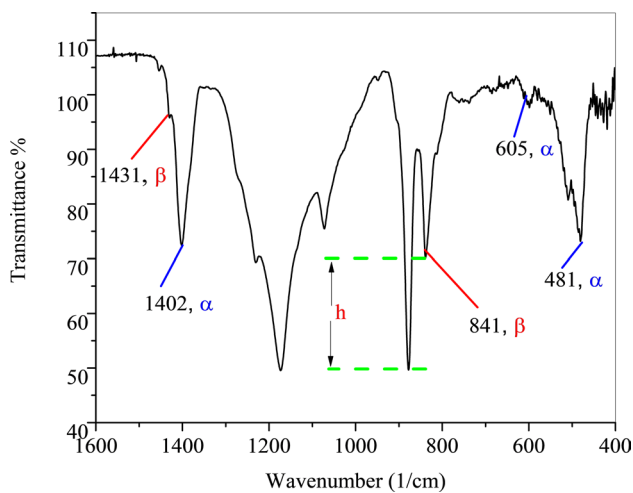


Fig. 1 FTIR of pure PVDF-HFP film

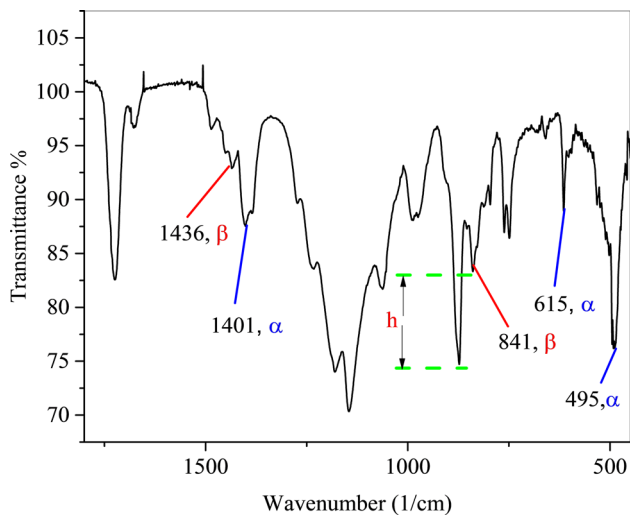


Fig. 2 FTIR of PVDF-HFP and PMMA blend film

When comparing the intensities of the peak at 1431 cm^{-1} and 1436 cm^{-1} in the two figure, it is clearly observed that incorporation of PMMA into the PVDF-HFP increased the absorption peak of β -phase. Two subsidiary dashed lines were used for determining the height between sharp peaks at 880 cm^{-1} and 840 cm^{-1} . The height between these two peaks were decreased 100% when PVDF-HFP was blended with PMMA. On the other words, β -phase was enhanced in the same ratio.

In Fig. 3, three different crystalline phases of PVDF-HFP were given. As mentioned, β -phase is the only electroactive crystalline form of PVDF-HFP. No clue for γ -phase was detected. The reason of the increase in β -phase content when blended was explained in terms of attraction between partially positive charged carbon atoms ($\delta^+\text{C}=\text{O}^{\delta-}$) and partially negative charged oxygen and fluoride ($\delta^+\text{C}-\text{F}^{\delta-}$) atoms. In

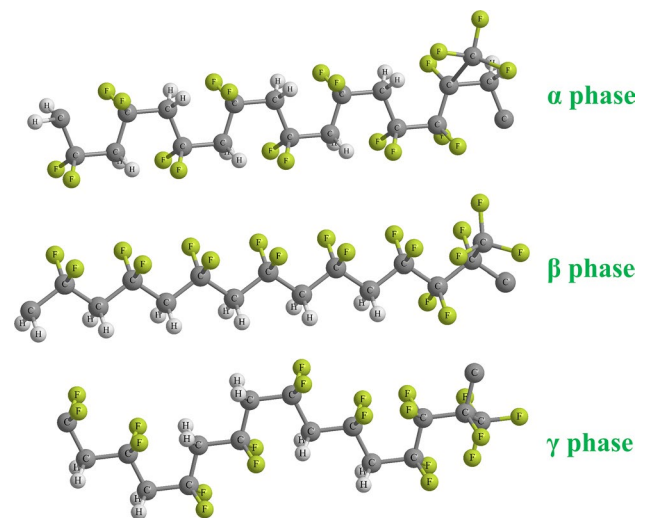


Fig. 3 Three different phase structure of PVDF-HFP

order to explain this concept more clearly, molecular models [40] were used In Fig. 4 where syndiotactic and isotactic isomers of PMMA are given. These two different molecular isomers are natural composition of any PMMA polymer.

Enhancement of β -phase content are considered to occur due to the influence of isotactic segments of PMMA in which a regular arrangement methacrylate groups induce the CF_2 groups to line up and enhance the existing β -phase content of PVDF-HFP as illustrated in Fig. 5.

Presence of α -phase which is electrically inactive phase of PVDF-HFP was also reasoned in the same manner. This phase does not produce piezoelectric voltage but existence of this phase must be kept at minimum. However, it is impossible to hinder the formation of α -phase due to the effect of syndiotactic segments of PMMA. Two regular arrays of methacrylate groups in opposite side of the backbone in syndiotactic PMMA induce the CF_2 groups to align in a trans position and enhance α -phase of PVDF-HFP as demonstrated in Fig. 6. In the two enhancement mechanisms, main molecular driving forces are the dipole–dipole interactions existing between CF_2 and $\text{C}=\text{O}$ groups.

3.2 Crystallinity and morphology by XRD and SEM

X-ray diffraction patterns for the PVDF-HFP and the blend films were given in Figs. 7 and 8. The peak at $2\theta = 17.5^\circ$ corresponds to the α -phase of pure PVDF-HFP with (020) miller indexed surface. A shoulder adsorption peak at $2\theta = 19.8^\circ$ belongs to the β -phase of pure PVDF-HFP with (110) and (200) miller indexed surfaces [41]. Upon blending with PMMA, it was observed that shoulder peak at $2\theta = 19.8^\circ$ which belongs to the β -phase was still well saved but due to the amorphous nature of PMMA, α -phase crystalline peak of PVDF-HFP at $2\theta = 17.5^\circ$ was hardly seen

Fig. 4 Two different tacticity in PMMA

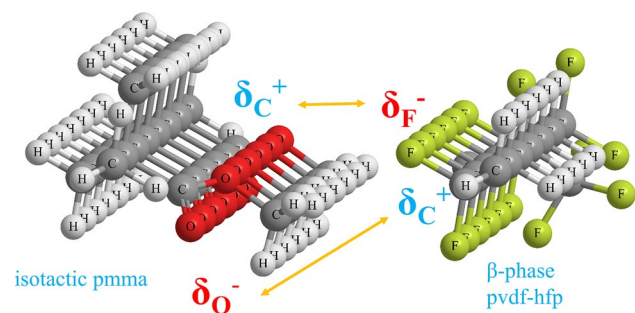
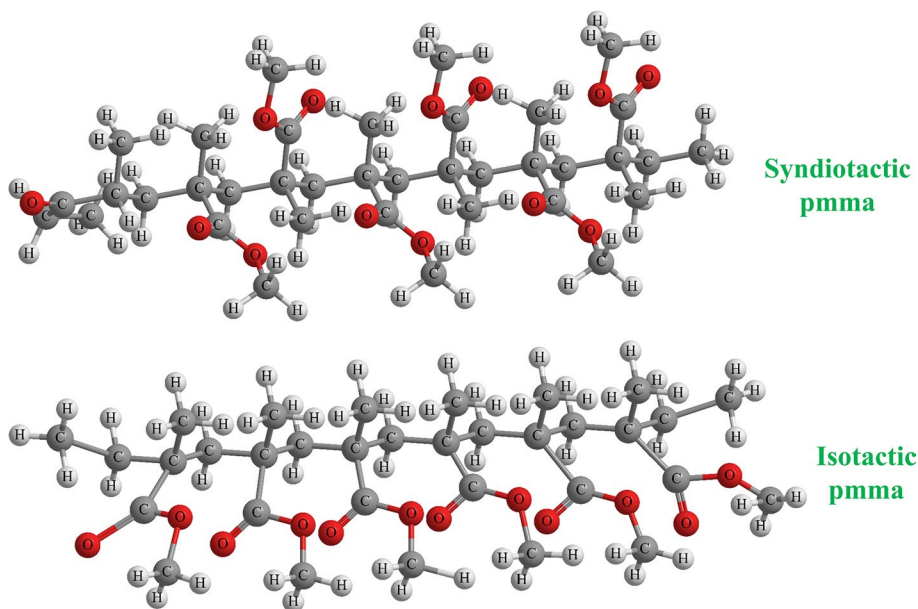


Fig. 5 Molecular model of β -phase enhancement of PVDF-HFP in the blend

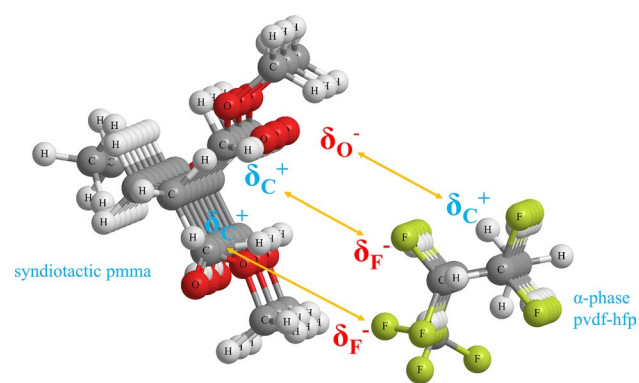


Fig. 6 Molecular model of α -phase formation of PVDF-HFP in the blend

with much reduced intensity because of broad peak between $2\theta=10^\circ$ and $2\theta=19^\circ$ as compared to the pure PVDF-HFP. However, some crystallinity of PMMA was inferred from

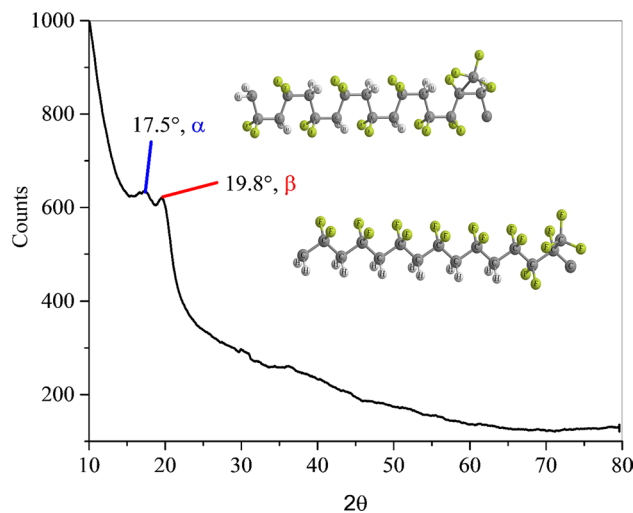


Fig. 7 XRD spectrum of pure PVDF-HFP

the peak observed at $2\theta=30.2^\circ$ [42]. The reason for preserving the β -phase peak $2\theta=19.8^\circ$ despite the dominating amorphous broad peaks of PMMA, can be attributed to the well coherence and attraction of the isotactic chain segments and CF_2 groups on the PVDF-HFP backbones as indicated in the Fig. 5.

SEM images of the pure PVDF-HFP (Fig. 9a, b) and the blend film (c, d) after spin coat process were given. Images were collected without gold coating. Uniformly distributed porous morphology was obtained with no micro crack. Thickness value was measured as $12\ \mu\text{m}$. Porous morphology might be an advantage for these films extending their uses for future applications. For instance, they might be used as voltage controlled membranes (or stimuli responsive

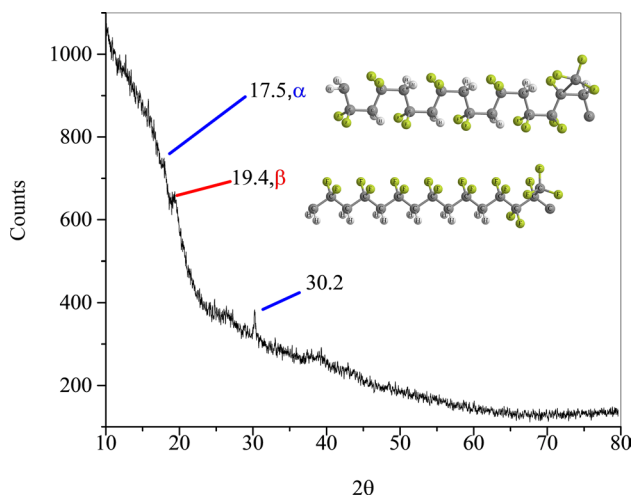


Fig. 8 XRD spectrum of the PVDF-HFP and blend film

membranes), where the pore size may be adjusted to desired levels by applying voltage.

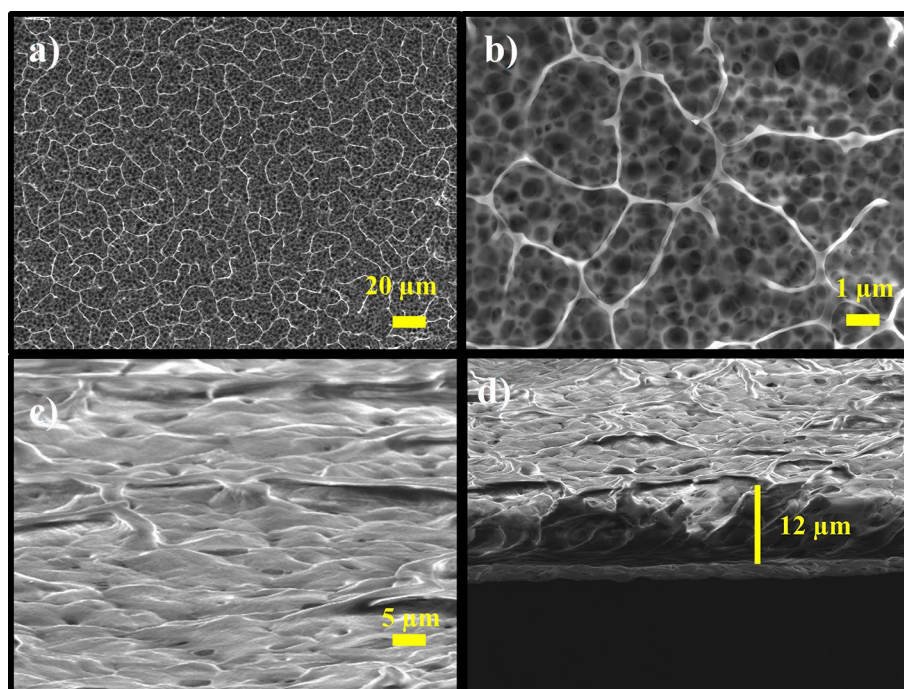
3.3 Thermal analysis by DSC and TGA

Differential scanning calorimeter (DSC) cooling thermograms were given in Fig. 10. Crystallization point (T_c) of PVDF-HFP was detected at 140 °C. Glass transition temperature (T_g), where the chain mobility starts and free volume between the chains begins to increase, was

determined at 59 °C. Incorporation of PMMA effects the DSC thermogram of the PVDF-HFP in the direction of reducing crystallization temperature from 140 to 129 °C. Approximately 7% decrease in the crystallization point can be attributed PMMA wrapped PVDF-HFP chains due to molecular attractions as indicated in Figs. 5 and 6. As seen from the DSC thermograms, glass transition temperature of PVDF-HFP at 59 °C disappears and merge into a new glass transition temperature at 94 °C [43]. This glass transition temperature is exactly equals to the T_g of amorphous PMMA as expected. It shows that PMMA and PVDF-HFP chains makes movements jointly. T_g of the polymers practically identify the softening point where the polymer loses its mechanical strength. Increasing the value of T_g from the 59 to 94 °C will be an advantage for diversifying its applications where high temperature mechanical durability together with piezoelectricity is desired.

Thermogravimetric percentage weight losses with their first derivative curves of the pure PVDF-HFP and blend films were given in Figs. 11 and 12. Maximum degradation rate temperature was found at 466 °C and took place in one step for the PVDF-HFP film. After blending with PMMA maximum degradation temperature was increased to 477 °C as given in Fig. 12. Although there is no huge increase, 2.3% heat stability were donated by PMMA. In the blend membrane, peaks at 293 °C and 368 °C correspond to the step wise chain scission processes in the PMMA thermal decomposition under nitrogen atmosphere [44].

Fig. 9 SEM images of the spin coated films **a, b** pure PVDF-HFP, **c, d** blend film



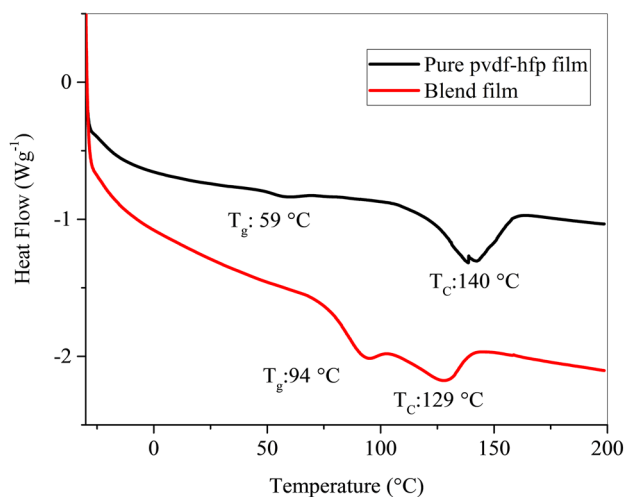


Fig. 10 DSC spectrum of the pure PVDF-HFP and blend film

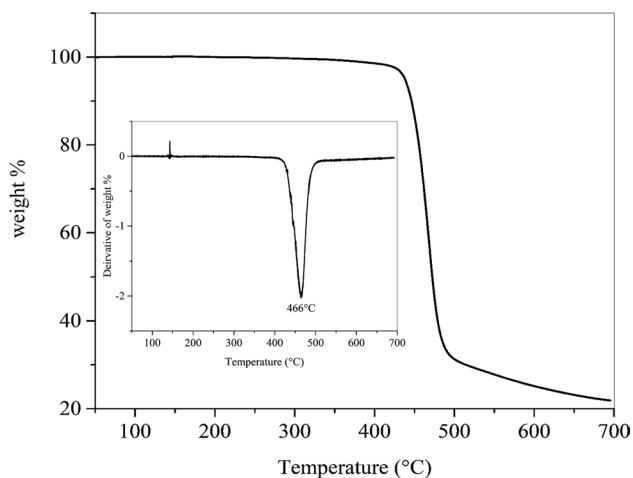


Fig. 11 TGA spectrum of pure PVDF-HFP film

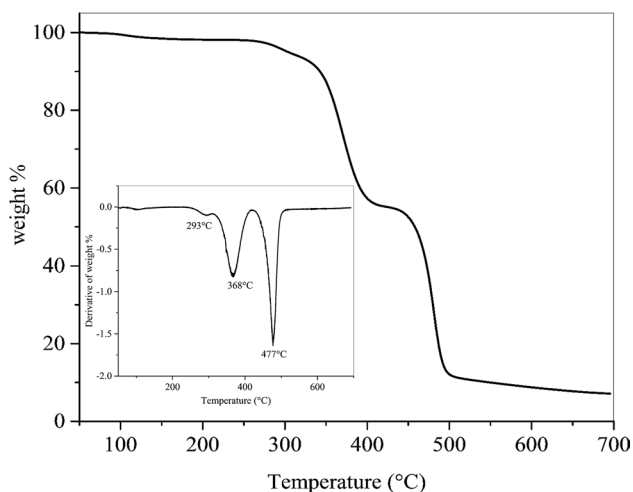


Fig. 12 TGA spectrum of the PVDF-HFP and blend film

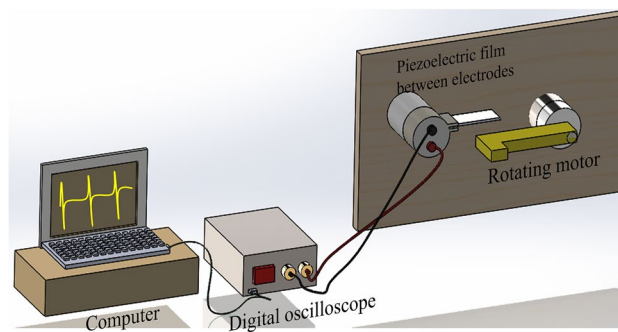


Fig. 13 Piezoelectric measurement setup

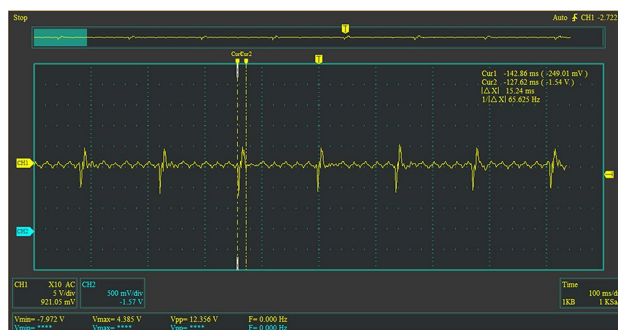


Fig. 14 Piezoelectric response of pure PVDF-HFP

3.4 Piezoelectric response

Piezoelectric response of the films was measured by a hand-made setup as introduced schematically in Fig. 13. A rotating plastic bar on the motor spindle hits the piezoelectric film which was sandwiched between two conducting ($2.5 \times 2.5 \text{ cm}^2$ area) aluminum electrodes. Produced signal was processed in a digital oscilloscope connected to a computer.

Signal collected for pure PVDF-HFP film was introduced in Fig. 14. Maximum voltage was determined as 4.385 V and peak to peak voltage was measured as 12.356 V. Produced voltage became zero at 15.24 ms after the force applied by plastic bar was removed. In Fig. 15 piezoelectric response of the blend film was shown. As seen, produced voltage by the film was 8.101 V which is almost two times greater than the pure PVDF-HFP film's voltage. Turning to zero potential or recovering the zero force conditions took 16.9 ms. Peak to peak voltage was found as 25.818 V. This results showed that β -phase enhancement was successfully done by addition of PMMA and spin coating technique was very useful to produce piezoelectric materials without needing poling procedure under high voltage conditions.

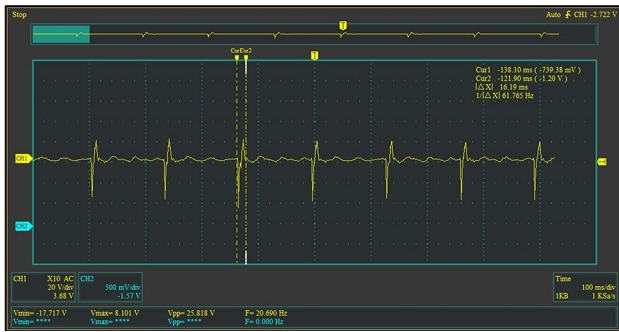


Fig. 15 Piezoelectric response of blend film

4 Conclusions

In this study, spin coated PVDF-HFP and a blend film with PMMA were prepared and compared. A detailed characterization was carried out to identify the changes in the crystal phase and thermal properties. FTIR results showed an increase in β -phase content and it was also supported by XRD patterns. Amorphous nature of PMMA hindered the α -phase peak but not cover the β -phase peak due to the well attraction between isotactic segments and CF_2 groups. In the Thermogravimetric analysis, PMMA showed three different decomposition region and all of which was related to its step wise chain scissions. Blending with PMMA increased the thermal stability of PVDF-HFP from 466 to 477 °C. DSC thermogram of the polymers demonstrated that crystallization temperature of the blend film decreased from 140 to 129 °C. Glass transition temperature of the PVDF-HFP seen at 59 °C disappeared and shifted to 94 °C when blended with PMMA. SEM images revealed a uniformly dispersed porous morphology. Thickness value was determined as 12 μm . Piezoelectric potential produced upon mechanical force was 4.385 V for PVDF-HFP and 8.101 V for the blend film. According to the results reached in this study addition of PMMA into the PVDF-HFP and spin coated technique was very useful and produced 84.7% increase in the piezoelectric potential. The blend film introduced in this study could be a good material for energy harvesting applications.

References

1. S. Priya, D.J. Inman (eds.), *Energy Harvesting Technologies* (Springer, Boston, 2009)
2. A. Harb, *Renew. Energy* **36**, 2641 (2011)
3. A. Ghaffarinejad, J. Yavand Hasani, *Appl. Phys. A* **125**, 259 (2019)
4. K. Xia, Z. Zhu, H. Zhang, Z. Xu, *Appl. Phys. A* **124**, 520 (2018)
5. S.-Y. Yang, J.-F. Shih, C.-C. Chang, C.-R. Yang, *Appl. Phys. A* **123**, 128 (2017)
6. A. Misra, R. Singh, S.P. Lal, *Appl. Phys. A* **121**, 597 (2015)
7. H.S. Kim, J.-H. Kim, J. Kim, *Int. J. Precis. Eng. Manuf.* **12**, 1129 (2011)
8. B. Bagchi, S. Banerjee, A. Kool, P. Thakur, S. Bhandary, N. Amin Hoque, S. Das, *Phys. Chem. Chem. Phys.* **18**, 16775 (2016)
9. M. Baniasadi, Z. Xu, S. Hong, M. Naraghi, M. Minary-Jolandan, A.C.S. *Appl. Mater. Interfaces* **8**, 2540 (2016)
10. K. R. Chapagain, W. Bjerke, S. Wagle, T. Melands, F. Melands, in *2017 IEEE International Ultrasonics Symposium IUS* (2017), pp. 1–4.
11. J. Chen, J. Zhao, L. Lin, X. Sun, *IEEE Sens. J.* **20**, 113 (2020)
12. A. Eddiai, M. Meddad, R. Farhan, M. Mazroui, M. Rguiti, D. Guyomar, *Superlattices Microstruct.* **127**, 20 (2019)
13. J. Gu, H. Yang, F. Fan, M. Su, *J. Instrum.* **12**, P12026 (2017)
14. W.G. Kaval, R.A. Lake, R. A. Coutu, in *Micro Nanomechanics*, vol. 5, ed. by L. Starman, J. Hay (Springer International Publishing, Cham, 2018), pp. 11–17
15. J. Ma, Q. Zhang, K. Lin, L. Zhou, Z. Ni, *Mater. Res. Express* **5**, 035057 (2018)
16. K.A.R. Medeiros, E.Q. Rangel, A.R. Sant'Anna, D.R. Louzada, C.R.H. Barbosa, J.R.M. d'Almeida, *Oil Gas Sci. Technol. Rev. D'IFP Energ. Nouv.* **73**, 48 (2018)
17. A.S. Motamedi, H. Mirzadeh, F. Hajiesmaeilbaigi, S. Bagheri-Khoulenjani, M.A. Shokrgozar, *J. Biomed. Mater. Res. A* **105**, 1984 (2017)
18. B. Qi, Q. Kong, H. Qian, D. Patil, I. Lim, M. Li, D. Liu, G. Song, *Sensors* **18**, 671 (2018)
19. S. Abbrent, J. Plestil, D. Hlavata, J. Lindgren, J. Tegenfeldt, Å. Wendsjö, *Polymer* **42**, 1407 (2001)
20. G. Kang, Y. Cao, *J. Membr. Sci.* **463**, 145 (2014)
21. A. Manuel Stephan, *Eur. Polym. J.* **42**, 21 (2006)
22. L. Wu, W. Yuan, N. Hu, Z. Wang, C. Chen, J. Qiu, J. Ying, Y. Li, *J. Phys. Appl. Phys.* **47**, 135302 (2014)
23. L. Ruan, X. Yao, Y. Chang, L. Zhou, G. Qin, X. Zhang, *Polymers* **10**, 228 (2018)
24. S. Ramasundaram, S. Yoon, K.J. Kim, C. Park, *J. Polym. Sci. Part B Polym. Phys.* **46**, 2173 (2008)
25. H.C. Bidsorkhi, A.G. D'Aloia, G. De Bellis, A. Proietti, A. Rinaldi, M. Fortunato, P. Ballirano, M.P. Bracciale, M.L. Santarelli, M.S. Sarto, *Mater. Today Commun.* **11**, 163 (2017)
26. J. Cai, N. Hu, L. Wu, Y. Liu, Y. Li, H. Ning, X. Liu, L. Lin, *Compos. Part Appl. Sci. Manuf.* **121**, 223 (2019)
27. C. Chen, F. Cai, Y. Zhu, L. Liao, J. Qian, F.-G. Yuan, N. Zhang, *Smart Mater. Struct.* **28**, 065017 (2019)
28. A.L. Gayen, D. Mondal, D. Roy, P. Bandyopadhyay, S. Manna, R. Basu, S. Das, D.S. Bhar, B.K. Paul, P. Nandy, *J. Mater. Sci. Mater. Electron.* **28**, 14798 (2017)
29. K. Huang, H. Ning, N. Hu, X. Wu, S. Wang, S. Weng, W. Yuan, L. Wu, Y. Liu, *Carbon* **144**, 509 (2019)
30. D. Mondal, A.L. Gayen, B.K. Paul, P. Bandyopadhyay, D. Bera, D.S. Bhar, K. Das, P. Nandy, S. Das, *J. Mater. Sci. Mater. Electron.* **29**, 14535 (2018)
31. H. Parangusan, D. Ponnamma, M.A.A. Al-Maadeed, *Sci. Rep.* **8**, 1 (2018)
32. W.-W. Cui, D.-Y. Tang, Y.-S. Lu, N. Zhang, L.-Z. Liu, J.-L. Mu, *Iran. Polym. J.* **26**, 179 (2017)
33. C.-H. Du, B.-K. Zhu, Y.-Y. Xu, *J. Mater. Sci.* **41**, 417 (2006)
34. J. Liu, M. Liu, C. He, J. Li, Q. Li, C. Wang, Y. Xi, *Ionics* **25**, 5201 (2019)
35. T. Ma, Z. Cui, Y. Wu, S. Qin, H. Wang, F. Yan, N. Han, J. Li, *J. Membr. Sci.* **444**, 213 (2013)
36. P. Senthil Kumar, A. Sakunthala, M.V. Reddy, M. Prabu, *Solid State Ion.* **319**, 256 (2018)
37. L.N. Sim, S.R. Majid, A.K. Arof, *Vib. Spectrosc.* **58**, 57 (2012)
38. B. Luo, X. Wang, H. Wang, Z. Cai, L. Li, *Compos. Sci. Technol.* **151**, 94 (2017)

39. G. Peng, X. Zhao, Z. Zhan, S. Ci, Q. Wang, Y. Liang, M. Zhao, *RSC Adv.* **4**, 16849 (2014)
40. C. Wan, C.R. Bowen, *J. Mater. Chem. A* **5**, 3091 (2017)
41. Q. Meng, W. Li, Y. Zheng, Z. Zhang, *J. Appl. Polym. Sci.* **116**, 2674 (2010)
42. I.S. Elashmawi, N.A. Hakeem, *Polym. Eng. Sci.* **48**, 895 (2008)
43. S.R. Valandro, P.C. Lombardo, A.L. Poli, M.A. Horn Jr., M.G. Neumann, C.C.S. Cavalheiro, *Mater. Res.* **17**, 265 (2014)
44. National Fire Protection Association and Society of Fire Protection Engineers (eds) *SFPE Handbook of Fire Protection*

Engineering, 3rd ed (National Fire Protection Association; Society of Fire Protection Engineers, Quincy, Mass.: Bethesda, Md, 2002)

Publisher's Note Springer Nature remains neutral with regard to jurisdictional claims in published maps and institutional affiliations.